PHYSICS OF FLUIDS **26**, 035101 (2014)

Estimating uncertainties in statistics computed from direct numerical simulation

Todd A. Oliver,[1,a)] Nicholas Malaya,[1,b)] Rhys Ulerich,[1,c)]
and Robert D. Moser[1,2,d)]
[1]*Center for Predictive Engineering and Computational Sciences, Institute for Computational Engineering and Sciences, The University of Texas at Austin, Austin, Texas 78712, USA*
[2]*Department of Mechanical Engineering, The University of Texas at Austin, Austin, Texas 78712, USA*

(Received 25 September 2013; accepted 5 February 2014; published online 6 March 2014)

Rigorous assessment of uncertainty is crucial to the utility of direct numerical simulation (DNS) results. Uncertainties in the computed statistics arise from two sources: finite statistical sampling and the discretization of the Navier–Stokes equations. Due to the presence of non-trivial sampling error, standard techniques for estimating discretization error (such as Richardson extrapolation) fail or are unreliable. This work provides a systematic and unified approach for estimating these errors. First, a sampling error estimator that accounts for correlation in the input data is developed. Then, this sampling error estimate is used as part of a Bayesian extension of Richardson extrapolation in order to characterize the discretization error. These methods are tested using the Lorenz equations and are shown to perform well. These techniques are then used to investigate the sampling and discretization errors in the DNS of a wall-bounded turbulent flow at $Re_\tau \approx 180$. Both small ($L_x/\delta \times L_z/\delta = 4\pi \times 2\pi$) and large ($L_x/\delta \times L_z/\delta = 12\pi \times 4\pi$) domain sizes are investigated. For each case, a sequence of meshes was generated by first designing a "nominal" mesh using standard heuristics for wall-bounded simulations. These nominal meshes were then coarsened to generate a sequence of grid resolutions appropriate for the Bayesian Richardson extrapolation method. In addition, the small box case is computationally inexpensive enough to allow simulation on a finer mesh, enabling the results of the extrapolation to be validated in a weak sense. For both cases, it is found that while the sampling uncertainty is large enough to make the order of accuracy difficult to determine, the estimated discretization errors are quite small. This indicates that the commonly used heuristics provide adequate resolution for this class of problems. However, it is also found that, for some quantities, the discretization error is not small relative to sampling error, indicating that the conventional wisdom that sampling error dominates discretization error for this class of simulations needs to be reevaluated. [http://dx.doi.org/10.1063/1.4866813]

I. INTRODUCTION

Direct numerical simulation (DNS) of turbulence is a valuable tool for the study of turbulent flows. Statistical quantities computed from DNS results are commonly used both to further understanding of flow physics and test hypotheses regarding turbulence[1–3] as well as to calibrate and validate engineering turbulence models.[4–8] DNS data are thus commonly used like experimental data. Therefore, as with experimental data, to have confidence in the interpretation of a DNS or in

[a)]Electronic mail: oliver@ices.utexas.edu
[b)]Electronic mail: nick@ices.utexas.edu
[c)]Electronic mail: rhys@ices.utexas.edu
[d)]Electronic mail: rmoser@ices.utexas.edu

the meaning of any comparison with DNS data, one must understand the uncertainty in that data. However, it is not common in the DNS literature to report these uncertainties because uncertainties in the data are generally not systematically evaluated. Instead, it is common for expert practitioners to determine grid spacing requirements, required simulation time, etc. based on a combination of knowledge gained from previous experience and observations of simulation outputs. The goal of this work is to improve upon this practice by providing a systematic method for estimating uncertainty in the statistics computed from DNS data.

Uncertainty estimation for DNS is an example of solution verification for the computed statistical quantities. The goal of solution verification is to ensure that numerical solutions of a mathematical model are sufficiently accurate approximations to the exact solution of the model.[9,10] Solution verification techniques for computational fluid dynamics (CFD) have been the topic of a large body of research.[11–13] The simplest techniques in this domain are based on Richardson extrapolation for estimating discretization error given a sequence of simulations on successively finer meshes. Richardson extrapolation is commonly used to estimate the leading order error in numerical results for both deterministic[11] and stochastic[14] problems, but it has not commonly been used for error estimation in DNS. Because the outputs of DNS are generally statistical quantities, the results are contaminated not only by discretization error but also by sampling error. Of course, this is true as well for inherently stochastic problems, but it does not appear to have been accounted for in applications of Richardson extrapolation for stochastic differential equations. By neglecting the sampling error, one implicitly assumes that it is small relative to the discretization error. However, since the goal of DNS is to resolve all relevant physical scales, it is generally expected that errors due to finite sampling are not negligible relative to discretization errors. Thus, simple methods for estimating discretization error that are common for other CFD calculations, like standard Richardson extrapolation, are not directly applicable to DNS, because the estimated discretization error is greatly affected by sampling error. The result is that, while systematic mesh resolution studies have been performed,[15] it is not common to actually estimate discretization error. The approach introduced here extends classical Richardson extrapolation to account for sampling uncertainty, thus alleviating these issues.

To accomplish this, one must be able to estimate sampling errors. Of course, if the data used to compute the statistics are samples from independent, identically distributed random variables, the central limit theorem allows easy estimation of the sampling error. However, the samples used to generate DNS statistics are drawn from a time history and/or spatial field and are generally not independent. To reduce the correlation, the samples used to compute statistics are sometimes taken "far" apart in time and then treated as independent.[15] While this procedure has intuitive appeal, it can lead to underestimated uncertainty if the snapshots are not sufficiently separated. Alternatively, if the snapshots are taken too far apart, it leads to fewer samples and larger sampling error.

Instead of restricting the samples in this way, it is preferable to use all the available data and account for correlations. One approach to accounting for the correlations in DNS statistics, which was proposed by Hoyas and Jiménez,[16] uses a sequence of "coarse grainings" of the data. However, our experience has been that it is difficult to automate this procedure because the presence of noise often requires both user intervention and interpretation.

A more promising approach based on direct estimation of the correlations in the data has been used to estimate sampling errors in many fields, including the weather and climate communities.[17,18] In this approach, the autocorrelation of the data, which is not known *a priori*, must be estimated from the data, which presents its own challenges. Here, we follow the work of Broersen[19,20] and fit autoregressive models from which the autocorrelation function is then computed.

Given an estimate of the sampling error, discretization errors are estimated using data from simulations with different resolution levels. As noted earlier, because sampling uncertainty is generally expected to be of the same magnitude as the discretization error, at least for grid spacing and time steps used for production DNS, standard Richardson extrapolation generally fails to correctly estimate the discretization error. Here, a Bayesian extension of the standard Richardson extrapolation that accounts for both statistical uncertainty and prior information (e.g., the expected asymptotic order of accuracy) is formulated. In this new approach, the discretization error model is equivalent to that used in standard Richardson extrapolation—i.e., it is assumed that the discretization error is

proportional to the resolution parameter (e.g., the grid spacing) raised to some constant power—but the parameters of this model are treated as random variables. The distributions of these random variables are inferred using Bayes' theorem. This Bayesian statistical formulation effectively regularizes the Richardson extrapolation problem to decrease the sensitivity of the estimated discretization error to finite sampling effects.

The performance of these estimators is tested using the Lorenz equations. They are then applied to the problem of assessing uncertainties in statistics from the DNS of incompressible, turbulent channel flow at $Re_\tau \approx 180$. The resulting discretization error estimates are assessed using a small domain case where it is feasible to run a simulation with twice the resolution of the nominal simulation, which is designed according to typical DNS heuristics.

For many quantities, including the mean velocity, Reynolds shear stress, and skin friction coefficient, the discretization error model is validated, meaning that its predictions agree with the observations at higher resolution. For these quantities, the model is then used to predict the discretization error present in a large domain simulation with resolution again set by the usual heuristics. The results demonstrate that, for these quantities, the discretization errors are small, generally much less than one percent. Thus, the usual mesh heuristics appear to be adequate. It should be pointed out however that the estimated discretization error is often similar to or larger than the estimated sampling error. This result violates the conventional wisdom that sampling error dominates, indicating that it is important to systematically estimate discretization error effects as well.

Unfortunately, for other quantities, including the streamwise velocity variance and the vorticity variances, our simple discretization error model is invalidated by the high resolution small domain simulation results. While the observed changes between the nominal and high resolution simulation are small, and so there is no indication that the nominal resolution is inadequate, this invalidation precludes the use of the model to predict the discretization error with any confidence. Thus, no discretization error estimates are presented for these quantities.

The remainder of the paper is organized as follows. The full error estimation methodology is presented in Sec. II, including the sampling error estimation (Sec. II A), the Bayesian Richardson extrapolation procedure (Sec. II B), and the illustrative Lorenz example (Sec. II C). Results for DNS of $Re_\tau = 180$ channel flow are given in Sec. III, and Sec. IV provides conclusions.

II. METHODOLOGY

This work addresses two major sources of uncertainty in statistics computed from DNS: finite sampling error and discretization error. The sampling error estimator is described briefly in Sec. II A. This estimate is then used in a Bayesian extension of Richardson extrapolation to determine probabilistic estimates of the discretization error and the exact value of the statistic of interest, as described in Sec. II B. To assess the characteristics of these procedures in a simple setting where different regimes can easily be explored, both estimators are used to evaluate simulations of the Lorenz equations in Sec. II C.

A. Sampling error

This section outlines a method for estimating the variance of a sample average computed from correlated data. To fix notation, let X denote a scalar flow quantity (e.g., a velocity component). Assume that the DNS produces a sample from a statistically stationary sequence of random variables $\{X_i\}$ for $i = 0, 1, \ldots$. Of course, the simulation can only run for finite time, so only the first N components of this sequence are known. The average of the N available samples,

$$\langle X \rangle_N = \frac{1}{N} \sum_{i=0}^{N-1} X_i,$$

is then an approximation of the true mean $\mu = E[X] = E[X_0]$, where $E[\,\cdot\,]$ is the expected value. Then, the sampling error e_N is simply the difference between the sample average and the true mean:

$$e_N \equiv \langle X \rangle_N - E[X].$$

Extensions of the central limit theorem (CLT) valid for sequences in which independence is approached for large separations, as is expected for turbulence time series, imply e_N converges to a normal distribution with zero mean as N becomes large. The variance of e_N is thus all that is required to completely characterize the sampling error. The estimator for the variance used here is motivated by this same generalization of the CLT, as described in the Appendix.

Following Trenberth,[17] the sampling error is estimated as

$$\operatorname{Var} e_N \approx \frac{\hat{\sigma}_N^2 T_0}{N}, \tag{1}$$

where

$$\hat{\sigma}_N^2 = \frac{1}{N - T_0} \sum_{i=0}^{N-1} (X_i - \langle X \rangle_N)^2, \tag{2}$$

and T_0 is the decorrelation separation distance. Specifically,

$$T_0 = 1 + 2 \sum_{k=1}^{N-1} \left(1 - \frac{k}{N}\right) \hat{\rho}(k), \tag{3}$$

where $\hat{\rho}$ is an estimate of the unknown true autocorrelation function ρ. The factor of $1 - k/N$ appears in (3) because the autocorrelation function must be estimated from data. In this case, a number of researchers have found that (3) gives lower mean-square error than the more obvious form in which the $1 - k/N$ is absent.[17,21,22] The expression (1) for $\operatorname{Var} e_N$ is the same as the estimate that would be obtained if $N_{\text{eff}} = N/T_0$ independent samples were used, making N_{eff} a measure of the effective size of a sample.

The fundamental challenge in estimating the variance of the sample average is the approximation of the autocorrelation ρ. While ρ can be approximated directly from the definition, such a naive approximation tends to be noisy, which can lead to bad estimates of T_0.[22] Obtaining a useful estimate of ρ requires more sophisticated techniques, especially for modest sample sizes. Here, we follow Storch and Zwiers[23] (Sec. 17.1.3) and fit an autoregressive (AR) time series model[24,25] to the observed sequence X_i. An AR process of order p takes the following form

$$X_n + a_1 X_{n-1} + \cdots + a_p X_{n-p} = \epsilon_n, \quad \epsilon_n \sim \mathcal{N}\left(0, \sigma_\epsilon^2\right), \tag{4}$$

where $\epsilon_n \sim \mathcal{N}(m, s^2)$ indicates that ϵ_n is a Gaussian random variable with mean m and variance s^2. AR processes are nothing but the output of an all-pole infinite impulse response filter driven by white noise input. The process parameters $a_1, \ldots, a_p$ and noise variance σ_ϵ^2 completely define the process, and thus, given these parameters, the exact autocorrelation function of the AR process may be computed.[20] This autocorrelation function is then used as $\hat{\rho}$ to compute T_0 according to (3).

Thus, estimating the autocorrelation reduces to estimating the parameters of an AR model. However, because the "true" process order is unknown, a hierarchy of models with increasing order p are simultaneously estimated.[19,20] From these candidates, the best model is chosen using an information-theoretic, finite sampling model selection criterion.[26]

Fitting such models to observed data has been studied extensively,[19,20,27–31] and there are a number of available algorithms. Here, classical Burg recursion[30] was used to fit models for various p, with Broersen's combined information criterion (CIC)[26] subsequently used to select the optimal p, although similar results have been obtained with other selection criteria. An open source, header-only C++ reference implementation is available at http://rhysu.github.com/ar/. Convenient wrappers for GNU Octave[32] and Python[33] are also provided. While this implementation is sufficient for the results shown in Secs. II C and III, it can fail due to accumulated round-off error in some circumstances. The reference implementation employs classical Burg recursion[30] specifically because it is less susceptible to round-off accumulation than the more efficient alternatives.[28,29] However, the authors

have observed that T_0 can be sensitive to accumulated round-off error when processing large synthetic data sets that have extremely low noise or very long decorrelation times relative to the sampling rate. Specifically, T_0 can be either non-convergent or artificially large. The former symptom is obvious when encountered. The latter can be detected by fitting the model using different working precisions, which is supported by the reference implementation.

B. Discretization error

In addition to the sampling error, discretization error contributes to the error in statistics computed from DNS. As part of a typical calculation, statistics computed from multiple levels of mesh resolution are available because course meshes are often used to speed convergence to a statistically stationary state. In principle, this information can be used to estimate discretization error. However, the standard procedure, Richardson extrapolation, does not account for sampling error, which can lead to misleading results. This procedure and issues introduced by sampling error are described in Sec. II B 1. An extension of this method that accounts for the sampling error through a Bayesian calibration procedure is described in Sec. II B 2.

1. Assessing order of accuracy without sampling error

Given simulations using at least three distinct resolutions, the convergence rate of a discrete approximation to an unknown continuum value may be assessed,[11,12] assuming that all three resolutions are in the asymptotic convergence range. Let q denote the exact value of some output quantity and q_h denote the discrete approximation of q at resolution level h. Assuming that

$$q - q_h = C_0 h^p + C_1 h^{p+1} + \cdots, \tag{5}$$

gives rise to the classical Richardson extrapolation procedure. The input data are a sequence of outputs q_{h_0}, q_{h_1}, and q_{h_2} resulting from computations for successively finer discrete approximations h_0, h_1, and h_2. Given this data and neglecting $O(h^{p+1})$ contributions, one can estimate the leading error order p by solving

$$\frac{q_{h_2} - q_{h_1}}{q_{h_1} - q_{h_0}} = r_1^p \frac{(r_2^p - 1)}{(r_1^p - 1)} \tag{6}$$

for p, where $r_1 = h_1/h_0$ and $r_2 = h_2/h_1$.

Unfortunately, when the computed discrete approximation is a statistical quantity that is contaminated by sampling error, this procedure can give misleading results. For instance, when the sampling error is large, the computed order p may be very far from the true p that would be obtained if sampling error were eliminated, making it appear that the discretization error is either much larger or much smaller than the true error. If the sampling error is large enough, it can make the implied p negative, making it appear that the solution is diverging. Or, Eq. (6) may have no solution at all, making it impossible to assess p or the discretization error. Thus, this procedure is insufficient when significant sampling error is expected.

2. Accounting for sampling error

To account for sampling error, a probabilistic model of the true mean that includes both the discretization error described in Sec. II B 1 and the sampling error estimate described in Sec. II A is needed. Using this model, the parameters of the discretization error model (e.g., the constants C_0 and p) are then estimated using Bayesian inference. This formulation is advantageous relative to a deterministic procedure (e.g., least-squares or maximum likelihood estimation) in the current context because it naturally assesses the uncertainty in the discretization error estimate, eliminating the flaw in the standard procedure described in Sec. II B 1. Since the Bayesian approach to inverse problems is described in more detail by many authors,[34–38] additional background information is omitted here.

To develop a probabilistic model for the true mean $E[q]$, let $e_{h,N}$ denote the sampling error for the sample average computed from N correlated samples at resolution h. That is,

$$e_{h,N} = E[q_h] - \langle q_h \rangle_N,$$

where $E[q_h]$ is the true mean at resolution h and $\langle q_h \rangle_N$ is the sample average computed from N samples. Further, letting $\epsilon_h = E[q] - E[q_h]$ denote the discretization error, we have

$$E[q] = \langle q_h \rangle_N + e_{h,N} + \epsilon_h. \tag{7}$$

Using the sampling error estimator from Sec. II A for $e_{h,N}$ and the form of ϵ_h from (5), one has a complete probabilistic model of the true mean $E[q]$. Specifically,

$$E[q] = \langle q_h \rangle_N + e_{h,N} + C_0 h^p + C_1 h^{p+1} + \ldots,$$

where $e_{h,N} \sim \mathcal{N}(0, \hat{\sigma}^2_{h,N})$ and $\hat{\sigma}_{h,N}$ is the estimate from (2) computed at resolution h. Note that, while $E[q]$ is a deterministic quantity, our knowledge of $E[q]$ is incomplete. Since Bayesian probability is a representation of incomplete knowledge, it is appropriate that $E[q]$ is represented by a probabilistic model. Neglecting the $O(h^{p+1})$ terms gives

$$E[q] - \langle q_h \rangle_N - C_0 h^p = e_{h,N} \sim \mathcal{N}(0, \hat{\sigma}^2_{h,N}). \tag{8}$$

This model forms the basis of the Bayesian inverse problem formulated later in this section, and we use it exclusively in this work. However, with appropriate modifications of the likelihood function defined below, any discretization error model may be used here in place of $C_0 h^p$. For instance, one could retain additional terms in the error expansion (5) to form different discretization error models.

For brevity, let $\bar{q} = E[q]$ from now forward. Then, given M sample averages $\hat{q}_i = \langle q_{h_i} \rangle_{N_i}$ $i = 1, \ldots, M$ computed using distinct mesh sizes h_i, Bayes' theorem implies that

$$\pi(\bar{q}, C_0, p | \hat{q}_1, \ldots \hat{q}_M) \propto \pi(\bar{q}, C_0, p)\, \pi(\hat{q}_1, \ldots, \hat{q}_M | \bar{q}, C_0, p), \tag{9}$$

where $\pi(a|b)$ denotes the probability density function (PDF) for a conditioned on b. The right hand side of (9) is composed of two factors: the prior PDF and the likelihood function. The prior PDF $\pi(\bar{q}, C_0, p)$ encodes any available information about the parameters $\bar{q}$, C_0, and p that is independent of the observations $\hat{q}_i$. For instance, one may have strong prior information regarding p because the formal order of accuracy of the numerical scheme is known. The likelihood function assesses the consistency of the model with particular values of the parameters $\bar{q}$, C_0, and p and the computed values $\hat{q}_1, \ldots, \hat{q}_M$. It is derived from the probabilistic model (7). Assuming that sampling errors for different resolutions h_i are independent,

$$\pi(\hat{q}_1, \ldots, \hat{q}_M | \bar{q}, C, p) = \prod_{i=1}^{M} \pi(\hat{q}_i | \bar{q}, C, p).$$

Then, from (8), it is clear that

$$\pi(\hat{q}_i | \bar{q}, C, p) = \frac{1}{\sigma_i} \phi\left(\frac{\bar{q} - \hat{q}_i - C h_i^p}{\sigma_i} \right),$$

where ϕ is the standard normal density $\phi(x) = \frac{1}{\sqrt{2\pi}} \exp\left(-\frac{1}{2}x^2\right)$, and $\sigma_i = \hat{\sigma}_{h_i,N_i}$.

Note that, for $M = 3$, as $\sigma_i \to 0$ the likelihood PDF approaches the δ distribution centered at the observed values, and thus, this Bayesian procedure reduces to the deterministic Richardson extrapolation approach described in Sec. II B 1.

To complete the specification of the Bayesian inverse problem, one must set priors on $\bar{q}$, C_0, and p. For simplicity, we take $\bar{q}$, C_0, and p to be independent in the prior. In principle, one could use a "non-informative" prior for these quantities. However, this would generally be inappropriate because the analyst often does have non-trivial prior information regarding the true value of the statistic, the plausible discretization error, and the order of accuracy. For instance, in the context of DNS, this information would come from similar simulations published in the literature as well as knowledge of the numerical methods being used. To allow this information to be incorporated, we

specify the priors as

$$\bar{q} \sim \mathcal{N}\left(q_0, \sigma_q^2\right) \qquad C \sim \mathcal{N}\left(0, \sigma_C^2\right) \qquad p \sim \text{Gamma}\left(\alpha, \beta\right), \tag{10}$$

where q_0, σ_q, σ_C, α, and β are parameters that define the specific prior PDF, and $p \sim \text{Gamma}(\alpha, \beta)$ indicates that p is a random variable with probability distribution given by the Gamma distribution:

$$\pi\left(p\right) = \frac{\beta^\alpha p^{\alpha-1}}{\Gamma(\alpha)} \exp\left(-\beta p\right) = \frac{\sqrt{2\pi}\beta^\alpha p^{\alpha-1}}{\Gamma(\alpha)} \phi\left(\sqrt{2\beta p}\right) \tag{11}$$

The parameter values used to generate results as well as the motivations for these values are given with the corresponding results (see Secs. II C 2 and III A).

Substituting these priors into (9) gives

$$\pi\left(\bar{q}, C, p \mid \hat{q}_1, \ldots, \hat{q}_N; q_0, \sigma_q, \sigma_C, \alpha, \beta\right) \propto \frac{\sqrt{2\pi}\beta^\alpha p^{\alpha-1}}{\sigma_q \sigma_C \Gamma(\alpha)} \phi\left(\frac{\bar{q} - q_0}{\sigma_q}\right) \phi\left(\frac{C}{\sigma_C}\right) \phi\left(\sqrt{2\beta p}\right) \prod_{i=1}^{M} \frac{1}{\sigma_i} \phi\left(\frac{\bar{q} - \hat{q}_i - C h_i^p}{\sigma_i}\right), \tag{12}$$

where the dependence on prior parameters q_0, σ_q, σ_C, α, and β has been noted. While the posterior PDF is simple to write down according the Bayes' theorem, working with this PDF can be difficult. In general it is not possible to compute statistics for the posterior analytically because the necessary integrals cannot be evaluated in closed form. Instead, it is common to use Markov chain Monte Carlo (MCMC) algorithms to sample the posterior.[39] In this work, we use a Python[33] implementation relying on the `emcee` implementation[40] of Goodman and Weare's affine invariant MCMC sampling technique.[41]

C. Illustrative example: The Lorenz equations

To illustrate the application of the sampling and discretization error estimation techniques discussed here, they are applied to estimates of the means computed from solutions of the Lorenz equations. The Lorenz equations are a system of three ordinary differential equations:

$$\frac{dx}{dt} = \sigma(y - x), \tag{13a}$$

$$\frac{dy}{dt} = x(\rho - z) - y, \tag{13b}$$

$$\frac{dz}{dt} = xy - \beta z. \tag{13c}$$

Depending on the values of the parameters σ, β, and ρ, the system exhibits chaotic behavior. The methods described in Secs. II A and II B are therefore applicable to estimating errors in statistical quantities, such as the mean of z, computed from discrete approximations. In the results presented here, the parameters are set to their typical values: $\sigma = 10$, $\beta = \frac{8}{3}$, $\rho = 28$.

1. Sampling error estimator performance

First, we examine the performance of the sampling error estimator. Aided by GNU Parallel,[42] we accomplish this with an ensemble of 10 000 Lorenz simulations using a 3rd-order Runge-Kutta time marching scheme with constant time step of $\Delta t = 0.001$. For each simulation, the initial condition is randomly selected and the solution is evolved for 500 time units. After this initial burn-in period, statistics are computed using four different averaging periods T and a number of time intervals Δt_s between samples.

The statistic of interest here is the mean of z. Thus, for each averaging period T and sampling interval Δt_s, the process described above gives an estimate of the mean of z as well as an estimate of the sampling error computed using the process described in Sec. II A. This set of data allows

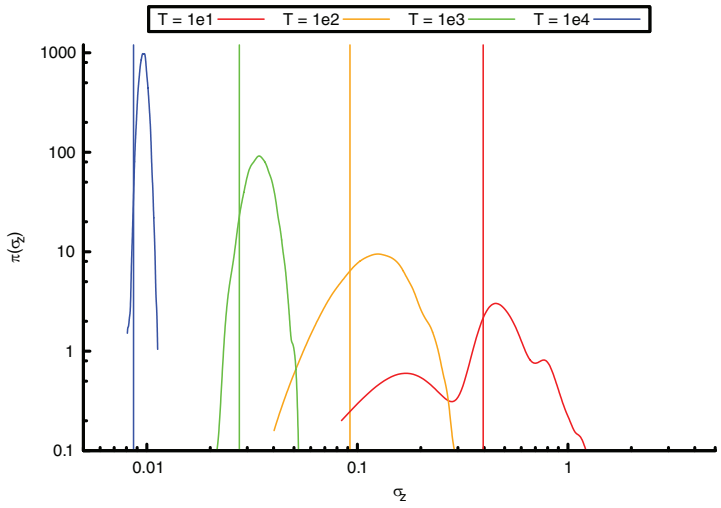

(a) $\Delta t_s = 0.1$

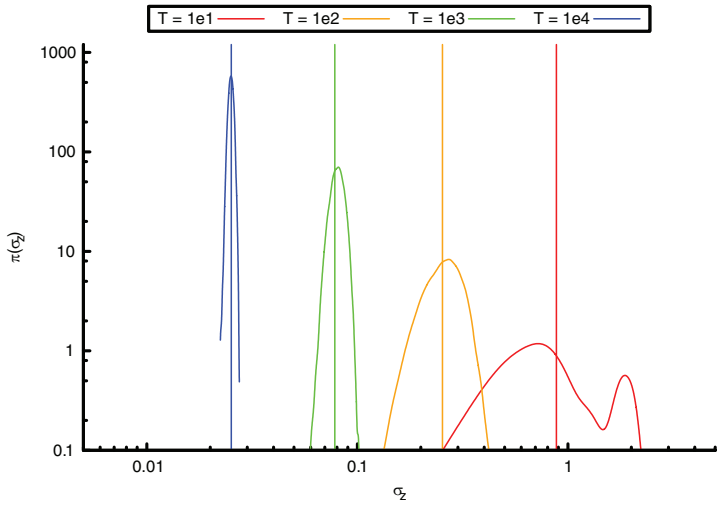

(b) $\Delta t_s = 0.5$

FIG. 1. PDFs of the standard deviation estimate for the sample average of z with various averaging periods T. Each estimate is computed according to (2), and the PDF is from a kernel density estimate computed from an ensemble of 10000 simulations of the Lorenz equations. For comparison, the empirically obtained σ_{true}, computed according to (14), are indicated by vertical lines.

comparison of the ensemble of sampling error estimates against the empirically observed standard deviation of the ensemble of estimates of the mean of z.

Figure 1 shows results of this comparison as T increases. Specifically, the figure shows the distribution of the estimated sampling error σ_z as well as an estimate of the "true" value of σ_z as determined from the ensembles of $\langle z_h \rangle_T$ values. That is,

$$\sigma_{\text{true}}^2 = \frac{1}{S-1} \sum_{i=1}^{S} \left(\mu_{\text{true}} - \langle z_h \rangle_{T,i} \right)^2, \tag{14}$$

where

$$\mu_{\text{true}} = \frac{1}{S} \sum_{i=1}^{S} \langle z_h \rangle_{T,i},$$

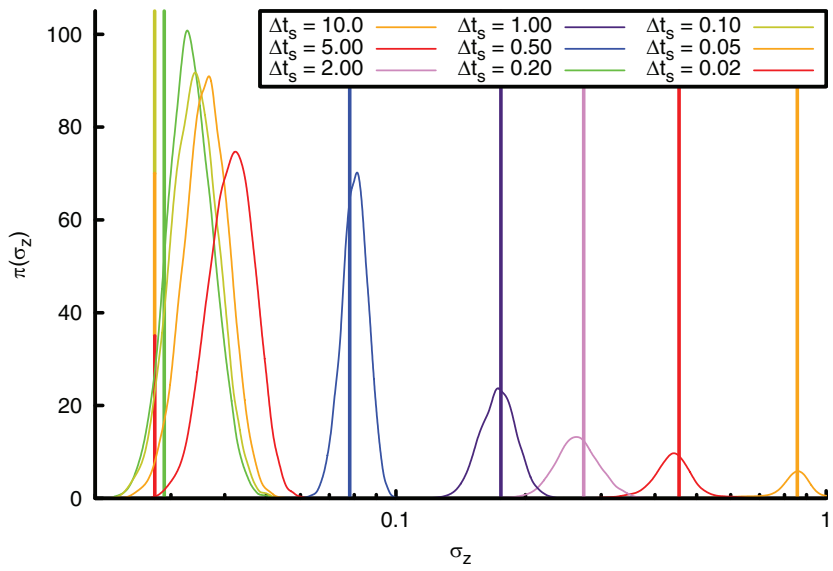

FIG. 2. PDFs of the standard deviation estimate for the sample average of z with various sampling interval Δt_s and an averaging duration $T = 1000$. Each estimate is computed according to (2), and the PDF is from a kernel density estimate computed from an ensemble of 10000 simulations of the Lorenz equations. For comparison, the empirically obtained σ_{true}, computed according to (14), are indicated by vertical lines.

$\langle z_h \rangle_{T,\,i}$ denotes the sample average of z for the ith simulation, and S is the total number of simulations in the ensemble.

In all cases, the estimated true value is within the support of the distribution of σ_z, indicating that the estimate is consistent with the true value. For $T = 10$, the PDF for σ_z has a multimodal shape with significant probability far from the estimated true value. This is due to the small sample size, which makes it difficult to accurately estimate the autocorrelation. As T increases, the probability density for the estimator clusters more tightly around the true value, and the results show the expected $\sigma_z \propto 1/\sqrt{T}$ scaling.

Figure 1 also shows a dependence of the estimated and observed statistical uncertainty on the sampling interval Δt_s. This dependence is explored further in Figure 2, which shows a larger range of Δt_s for fixed $T = 1000$. When Δt_s is large, the samples are less correlated. However, information is still discarded by neglecting even highly correlated samples, leading to larger uncertainty in the sample average of z. Beginning with large Δt_s, as Δt_s is decreased, the estimated σ_z and σ_{true} both decrease. However, for σ_z, this trend reverses for small enough Δt_s. While σ_{true} appears to converge, the estimated σ_z begins to grow when Δt_s become smaller than about 0.20. When Δt_s is less than about 0.01, the algorithm used to compute the σ_z breaks down due to the effects of round-off error. We hypothesize that the increase in σ_z with decreasing Δt_s below 0.20 is also due to accumulation of double precision round-off error. Repeating this study using both lower and higher floating point precision (not shown) produced behavior consistent with this hypothesis.

2. Bayesian Richardson extrapolation results

Here we explore the performance of the Bayesian Richardson extrapolation procedure described in Sec. II B in three regimes: small sampling error, medium sampling error, and large sampling error relative to the discretization error. In DNS, it is expected that sampling errors will generally be larger than or comparable to the discretization error. The small sampling error regime is also considered here for completeness.

Further, three numerical schemes are used: the RK3 method used to generate the results in Sec. II C 1 as well as forward Euler and the classical 4th order Runge-Kutta scheme. All parameters defining these simulations as well as the observed results for the sample average $\hat{q}$ and the estimated standard deviation of the sample average σ_z are shown in Table I. In all cases, the time between

TABLE I. Conditions and results for Lorenz simulations used in Bayesian Richardson extrapolation example.

Forward Euler						
	$T = 10^3$		$T = 10^5$		$T = 10^7$	
Δt	$\hat{q}$	σ_z	$\hat{q}$	σ_z	$\hat{q}$	σ_z
5×10^{-4}	23.6086	0.0307	23.6066	0.00250	23.6115	0.000247
2.5×10^{-4}	23.5916	0.0359	23.5812	0.00273	23.5802	0.000260
1.25×10^{-4}	23.5198	0.0333	23.5607	0.00269	23.5645	0.000268
RK3						
	$T = 10^3$		$T = 10^5$		$T = 10^7$	
Δt	$\hat{q}$	σ_z	$\hat{q}$	σ_z	$\hat{q}$	σ_z
2.5×10^{-2}	23.4535	0.0301	23.4822	0.00282	23.4762	0.000269
1.25×10^{-2}	23.5416	0.0388	23.5388	0.00285	23.5405	0.000275
6.25×10^{-3}	23.5281	0.0349	23.5501	0.00282	23.5487	0.000276
RK4						
	$T = 10^3$		$T = 10^5$		$T = 10^7$	
Δt	$\hat{q}$	σ_z	$\hat{q}$	σ_z	$\hat{q}$	σ_z
0.1	22.8586	0.0567	22.9764	0.00697	22.9703	0.000729
0.05	23.5054	0.0320	23.4858	0.00258	23.4889	0.000255
0.025	23.5635	0.0309	23.5486	0.00286	23.5489	0.000276

samples was $\Delta t_s = 0.1$, and the parameters for the prior are set as: $q_0 = 23.5$, $\sigma_q = 0.4$, $\sigma_C = 0.8$, $\alpha = 3$, $\beta = 1/2$.

The results of Bayesian Richardson extrapolation based on the data in Table I are shown in Figure 3. For each scheme and averaging period, the figure shows the marginal posterior PDFs for p, the observed order of accuracy, and q, the true value of the mean of z. When the averaging time duration is relatively short, such that the sampling error is large compared to the discretization error, the sampling error effectively masks the discretization error. In this case, the data contain little information about the true discretization error. Thus, the marginal posterior PDF for p is broad (essentially the same as the prior), and the true value of $\langle z \rangle$ cannot be inferred precisely. As more data are obtained, the posteriors for both p and q become increasingly sharp, indicating that the statistical uncertainty is small relative to the discretization error and that the Bayesian Richardson extrapolation is reverting to standard Richardson extrapolation. Note that for the forward Euler and RK3 discretizations, the expected asymptotic rates of $p = 1$ and $p = 3$, respectively, are obtained with very high confidence when the statistical uncertainty is sufficiently small. However, for the RK4 results, the probability for p clusters near $p \approx 3$ in the $T = 10^7$ case. This result indicates that the time step used here is not small enough for the results to be in the asymptotic convergence regime. However, if the time step is decreased further to get into the asymptotic regime, the sampling uncertainty for $T = 10^7$ is no longer sufficiently small to allow the order of accuracy to be determined with a high degree of certainty.

III. DNS OF $Re_\tau = 180$ CHANNEL FLOW

The techniques described in Sec. II have been used to investigate sampling and discretization errors in DNS of a wall-bounded turbulent flow. Specifically, we analyze DNS of fully-developed incompressible turbulent channel flow at bulk Reynolds number $Re_b = U_b \delta/\nu = 2925$, where U_b is the bulk velocity, ν is the kinematic viscosity and δ is the channel half-height. The corresponding friction Reynolds number is $Re_\tau = u_\tau \delta/\nu \approx 180$, where u_τ is the friction velocity. In the following, quantities are normalized by U_b and δ unless otherwise indicated. As is customary, a superscript $+$ indicates normalization in wall units; that is, normalization by u_τ and ν.

This relatively low Reynolds number case has been chosen to enable testing of the methods developed here because it is computationally tractable to simulate for times longer than usual, using higher resolution than usual. This allows the model predictions to be tested against observed

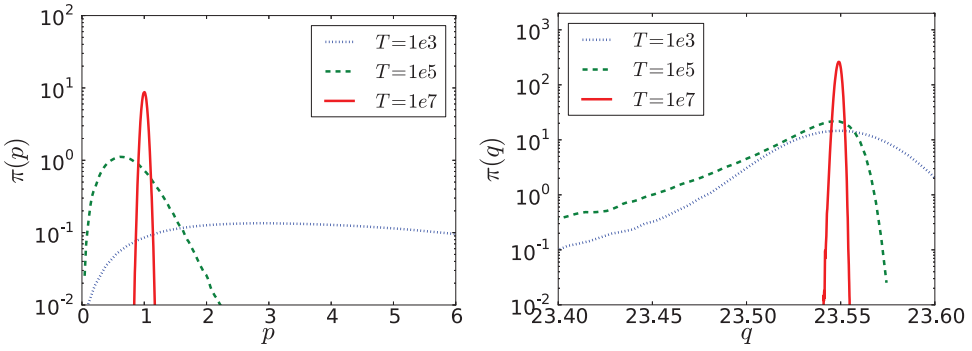

(a) Forward Euler.

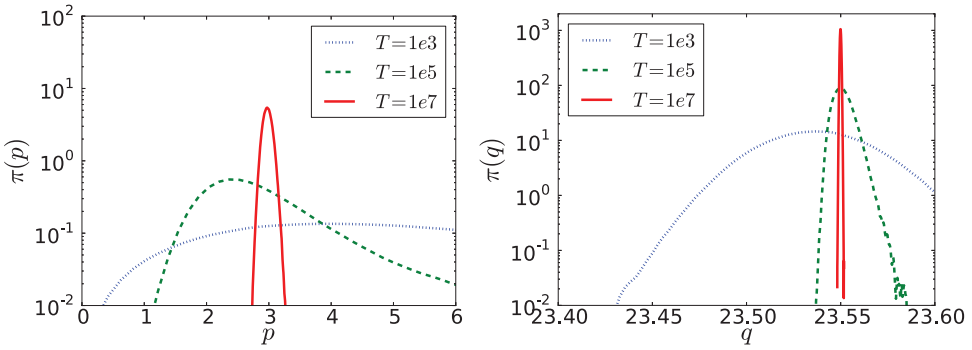

(b) RK3.

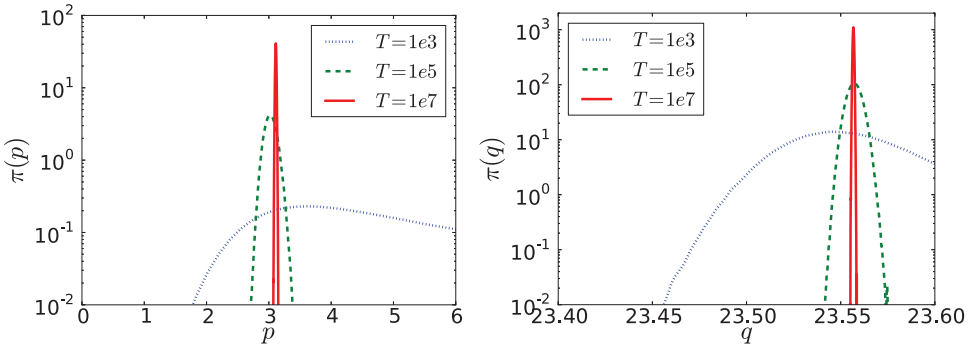

(c) RK4.

FIG. 3. Posterior distributions of the convergence order p and the quantity being estimated $q = \langle z \rangle$ from Bayesian Richardson extrapolation results for three different averaging durations T, which produce large ($T = 1e3$), similar ($T = 1e5$), and small ($T = 1e7$) statistical uncertainty compared to discretization error. Results are shown for three time discretizations of the Lorenz equations.

results, as shown in the small domain case. While this flow has been previously simulated by many authors,[43–45] and thus the results are not scientifically new, the characterization of the two error sources in DNS is novel. This characterization will provide insights relevant to DNS of wall-bounded flows in general. All of the data used in the Bayesian Richardson extrapolation, including computed statistics and estimated sampling errors, are available at http://turbulence.ices.utexas.edu.

A. Discretization, sampling, and prior details

The incompressible 3D Navier-Stokes equations are solved using the formulation of Kim, Moin, and Moser[43] (KMM), as implemented in the code developed by Lee *et al.*[46] This formulation involves integrating evolution equations for the wall-normal vorticity, ω_y, and the Laplacian of

the vertical velocity, $\nabla^2 v$. Periodic boundary conditions are imposed in the streamwise (x) and spanwise (z) directions while, in the wall normal direction (y), no slip conditions are imposed at the walls. A semi-implicit, third-order Runge–Kutta/Crank–Nicholson scheme is used for the time discretization.[47] The flow is driven by a spatially uniform pressure gradient that is adjusted in time to maintain a constant mass flux. Constraining the mass flux in this manner, as is commonly done, greatly reduces the required simulation time relative to using a constant-in-time pressure gradient because it eliminates a long time scale governing the relaxation of the flow to statistical stationarity. In space, a Fourier/Galerkin method is used in the streamwise and spanwise directions. Unlike KMM, a B-spline/collocation representation is used in the wall-normal direction because it allows for flexible non-uniform grids while retaining spectral-like resolution.[48] The B-spline breakpoints y_i for $i = 0, \ldots, N_b - 1$ are set in the interval $[-1, 1]$ according to

$$y_i = \frac{\sin\left(\frac{\alpha\pi}{2}\left[-1 + \frac{2i}{N_b - 1}\right]\right)}{\sin\left(\frac{\alpha\pi}{2}\right)}, \tag{15}$$

where N_b is the number of breakpoints and α is a stretching parameter, which is set to 0.985 for this study. The Greville abscissae, also called the Marsden–Schoenberg points, implied by these breakpoints[49,50] are used as the collocation points, of which there are $N_y = N_b + p_{\mathrm{bs}} - 1$, where p_{bs} is the B-spline order (7 in the simulations reported here). To develop Richardson extrapolation estimates, a nominal mesh resolution was defined, along with two uniform coarsenings (by factors of approximately $\sqrt{2}$ and 2), labeled "coarse" and "coarsest." The nominal mesh was designed to conform to resolution heuristics typically used in DNS of wall-bounded turbulence. That is, in x- and z-directions, $\Delta x^+ \approx 13$, $\Delta z^+ \approx 7$, where $\Delta x = L_x/N_x$ and $\Delta_z = L_z/N_z$ with N_x and N_z being the number of Fourier modes in the representation in the x and z directions, respectively. In the y-direction, the nominal mesh is required to have $\Delta y^+_{\mathrm{wall}} < 1$ at the walls and $\Delta y^+_{\mathrm{CL}} \approx \Delta z^+$ at the channel center, where Δy is the spacing between the break points.

A constant time step Δt was used in the simulations reported here. This is slightly different from typical DNS practice, in which variable time steps based on a Courant–Friedrichs–Lewy (CFL) condition[51] are used. Constant time steps are used here to ensure equidistant temporal samples, which simplify the temporal analysis required to estimate the sampling uncertainty. The time step size for the nominal mesh was selected by monitoring the time step in a CFL-based variable time-step calculation and choosing a step smaller than the smallest observed time step. Accordingly, these simulations are somewhat better resolved in time than is common practice. This analysis can be extended to adaptive timestepping by either managing the variable time step to ensure uniform samples in time—i.e., constant Δt between samples that are used to compute statistics—or by extending the autoregressive modeling approach to allow for non-equispaced samples.[52]

Two sets of DNS simulations were conducted: one using a relatively small domain with $L_x = 4\pi$ and $L_z = 2\pi$; the other in a larger domain with $L_x = 12\pi$ and $L_z = 4\pi$. The small domain size is that used by KMM, while the large domain is identical to that of the $Re_\tau \approx 180$ simulation reported by Hoyas and Jiménez.[53] The small domain case was studied because the simulations are less expensive, so that it was practical to perform a simulation with a finer grid than nominal (by a factor of 2, called "finest"), to allow validation of the Bayesian Richardson extrapolations. The large domain was simulated because the error estimates for this case will be relevant to the interpretation of the reference simulation results of Hoyas and Jiménez.[53] For each case, the simulation was run until a statistically stationary state was reached, and then statistics were collected over an evolution time T, with a sampling period of $0.1L_x/U_b$ or 10 samples per flow-through. The numerical parameters for each simulation are given in Table II.

The parameters defining the prior PDFs (10) used in the Bayesian Richardson extrapolation procedure are the same for both the small and large domain results. For $\bar{q}$, q_0 is taken from the $Re_\tau \approx 180$ channel flow simulation of del Álamo and Jiménez.[44,45] The standard deviation σ_q is taken as 2.5% of q_0, indicating that we expect the results of the del Álamo and Jiménez simulation to be within ±5% of the true values with approximately 95% confidence. While such strong prior information is not always available—i.e., one may not have a previous simulation of the same case—

TABLE II. Numerical and sampling parameters for turbulent channel flow simulations conducted at $Re_b = 2925$, $Re_\tau \approx 180$. Variables are as defined in Sec. III A.

Name	L_x	L_z	N_x	N_z	N_y	Δx^+	Δz^+	Δy^+_{wall}	Δy^+_{CL}	TU_b/L_x	$\Delta t U_b/\delta$
					Small domain						
Coarsest	4π	2π	96	96	64	24.3	12.2	0.51	10.10	2651.0	0.02
Coarse	4π	2π	136	136	90	17.2	8.6	0.29	6.94	273.5	0.01414
Nominal	4π	2π	192	192	128	12.2	6.1	0.17	4.76	2145.3	0.01
Finest	4π	2π	384	384	256	6.1	3.0	0.07	2.31	709.3	0.005
					Large domain						
Coarsest	12π	4π	256	192	64	27.4	12.2	0.51	10.10	40.0	0.02
Coarse	12π	4π	362	270	90	19.4	8.7	0.29	6.94	30.0	0.01414
Nominal	12π	4π	512	384	128	13.7	6.1	0.17	4.76	20.0	0.01

some information regarding the expected results is almost always available and should be included in the prior for $\bar{q}$.

The value of σ_C is taken to be $4\sigma_q$. Since h is normalized such that $h = 1$ on the coarsest mesh, σ_C represents an *a priori* estimate of the discretization error on the coarsest mesh. Choosing $4\sigma_q$ with σ_q set to 2.5% of $\bar{q}$ thus gives approximately 95% confidence that the discretization error on the coarsest mesh is less that $\pm 20\%$ of q_0.

Finally, we take $\alpha = 3$ and $\beta = 1/2$, which gives reasonable probability to a wide range of p values. This uncertainty is reasonable given the mix of orders in the complete discretization as well as the uncertainty about which part of the discretization error is dominant.

B. Small domain results

The Bayesian Richardson extrapolation procedure has been applied to a variety of statistical quantities of particular interest in the channel flow. For brevity, we show full results, including details of the joint posterior PDF for the true value $\langle q \rangle$, the discretization error constant C, and the order of accuracy p, for only two scalars: the centerline mean velocity and the skin friction coefficient. A summary of results for single-point statistics including the mean velocity, the Reynolds stresses, and the vorticity correlations at multiple points across the channel is also given. In all cases, the inverse problem is formulated using data from the coarsest, coarse, and nominal mesh resolutions. Data from the finest mesh are reserved to provide a validation test of the procedure.

1. Centerline mean velocity

The results of Bayesian Richardson extrapolation applied to the centerline mean velocity U_{CL} are presented here. First, we examine the results of the inverse problem for the discretization error model. Then, we test the calibrated model by using the model to predict the value that should be observed on the finest mesh. Finally, we use the model to examine the discretization error on the nominal mesh.

Figure 4 shows the posterior PDF for the calibration parameters. The posterior PDF for p is maximum near $p = 5$. While this does not correspond directly to any of the schemes used here, there is large uncertainty about the order, with the first and third quartiles of the marginal distribution for p at approximately 4.4 and 7.4, respectively. Despite the large uncertainty about the order of accuracy, the uncertainty regarding the true value is quite small. For instance, the difference between the 5th and 95th percentiles is less than 0.08% of the mean value.

Given the samples from the posterior PDF represented in Figure 4, one can use the calibrated model to make predictions of the value of the average centerline velocity that should be observed for any value of the resolution parameter h by evaluating

$$\langle q_h \rangle_N = E[q] - C_0 h^p - e_{h,N}. \tag{16}$$

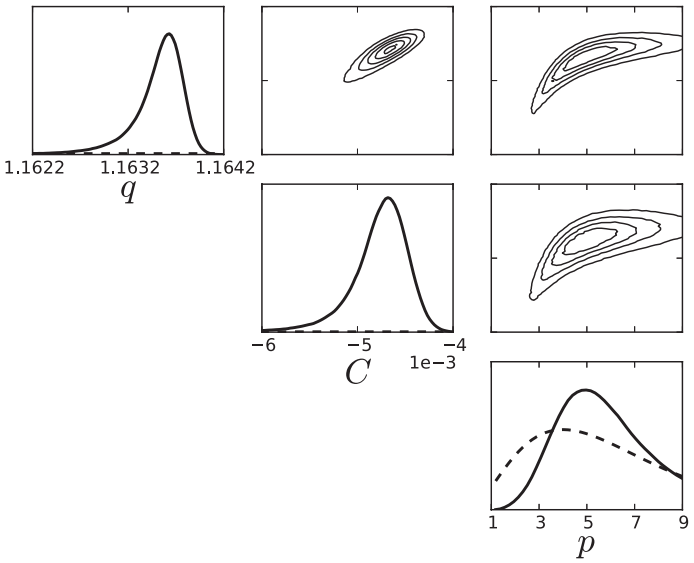

FIG. 4. Results of Bayesian Richardson extrapolation for $q = U_{CL}$, C, and p. The input data are U_{CL} from the coarsest, coarse, and nominal meshes for the small domain case. The diagonal shows the marginal prior (dashed line) and posterior (solid line) PDFs for each of the parameters while the off-diagonal contour plots show the joint posterior PDF projected onto planes in parameter space.

Here $e_{h,N}$ is the sampling uncertainty for the simulation from which the observed average velocity is obtained. Thus the distribution for $\langle q_h \rangle_N$ obtained from (16) includes uncertainty from two sources. First, the calibrated discretization error model parameters ($E[q]$, C_0, and p) are uncertain. Second, the observation is contaminated by sampling error. The consistency of the model with the actual observation can be assessed by simply examining whether the observed value is a plausible draw from the prediction distribution generated according to (16). If the observed value is highly unlikely according to the prediction, the model is declared invalid.

Results of this validation check for the centerline velocity are shown in Figure 5. Clearly, the observed value is not near the tail of the prediction distribution, indicating that there is no reason to believe the model is invalid. In particular, Figure 5(b) shows the cumulative distribution function (CDF) for the prediction. The prediction CDF evaluated at the actual observed value on the finest mesh is approximately 0.88. In Sec. III B 3, the prediction CDF evaluated at the observed value on the finest mesh will be used to assess the validity of the discretization error model.

Finally, Figure 6 shows the estimated discretization error on the nominal mesh, normalized by the observed mean value. Note that the discretization error is very small. Essentially all of the probability is assigned to values of less than 0.1%, and half is assigned to values less than 0.008%.

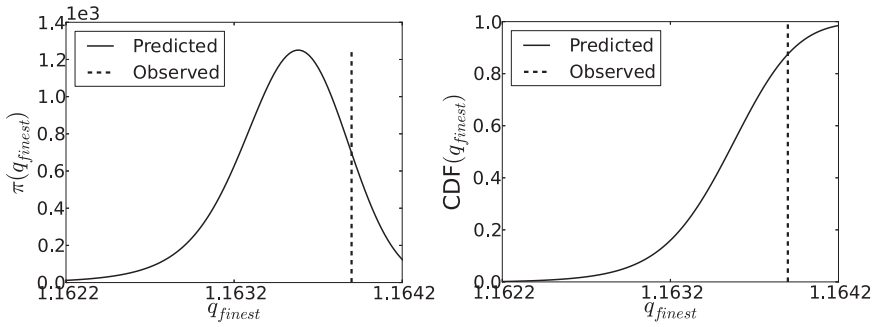

(a) PDF (b) CDF

FIG. 5. Prediction distribution of the mean centerline velocity for the finest mesh using (16) and the observed mean centerline velocity computed on the finest mesh for the small domain case. (a) PDF (b) CDF.

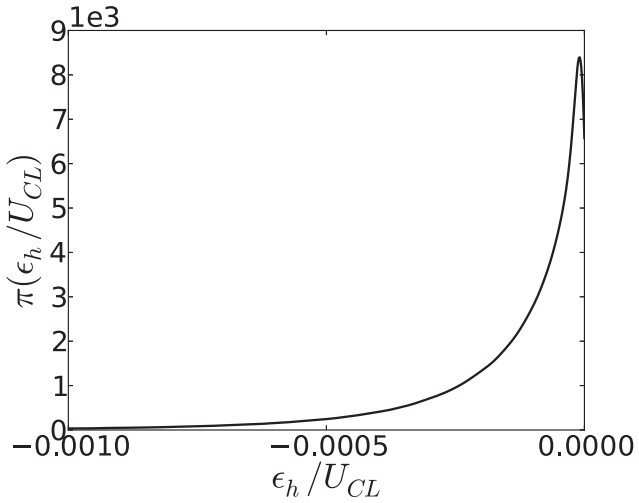

FIG. 6. Distribution of estimated discretization error in the centerline velocity on the nominal mesh for the small domain case, as determined by Bayesian Richardson extrapolation.

For comparison, the standard deviation of the sampling error was estimated as 0.011% for this mesh. Thus, even after more than 2000 flow-throughs, sampling uncertainty is still significant for this quantity.

Note that the discretization error distribution in Figure 6 has an odd shape, with high probability assigned to negative values very close to zero, but zero probability assigned to positive values. Similar distributions are observed in the results shown in subsequent sections for other quantities as well. This feature can be understood by examining the posterior distribution shown in Figure 4. Specifically, the value of C is bounded away from zero. Since $\epsilon_h = Ch^p$, C is the only parameter that can change the sign of ϵ_h. Since it is bounded away from zero, the model is completely sure of the sign of the discretization error. This result for C is entirely consistent with monotonic data with sampling uncertainty that is small relative to the changes observed between different resolution simulations. In this case, one should be able to determine the sign of the discretization error with very high confidence.

This explains why the discretization error tends to have all its probability on one side of zero, but we also observe that the probability density is highest near zero. This feature results from the fact that p is not well-informed. In particular, examining Figure 4, two features are apparent. First, large values of p are not ruled out by the data. Second, for large p, the most likely values of C are not sensitive to p (i.e., C is not increasing significantly as p increases). For constant C, larger values of p imply smaller values of ϵ_h, since $h < 1$. These features of the joint distribution for C and p cause the probability for ϵ_h to cluster near zero.

2. Skin friction

Results for the skin friction coefficient are analyzed here in a series of figures analogous to those shown for the centerline mean velocity. To begin, Figure 7 shows the joint posterior PDF for the parameters of the discretization error model. While the order of accuracy appears somewhat better informed than for the centerline velocity, there is still significant uncertainty, with the 5th and 95th percentiles at 3.07 and 5.29, respectively. However, the marginal posterior for the true value of C_f is again quite narrow, with the difference between the 5th and 95th percentiles being only 0.54% of the mean value.

Figure 8 compares the model prediction of the skin friction on the finest mesh, computed from the calibrated discretization error model and the estimated sampling uncertainty in the finest mesh result using (16), and the observed results. Clearly, there is good agreement between the prediction and the observation. As with the centerline velocity, there is no reason to question the discretization error model in this case.

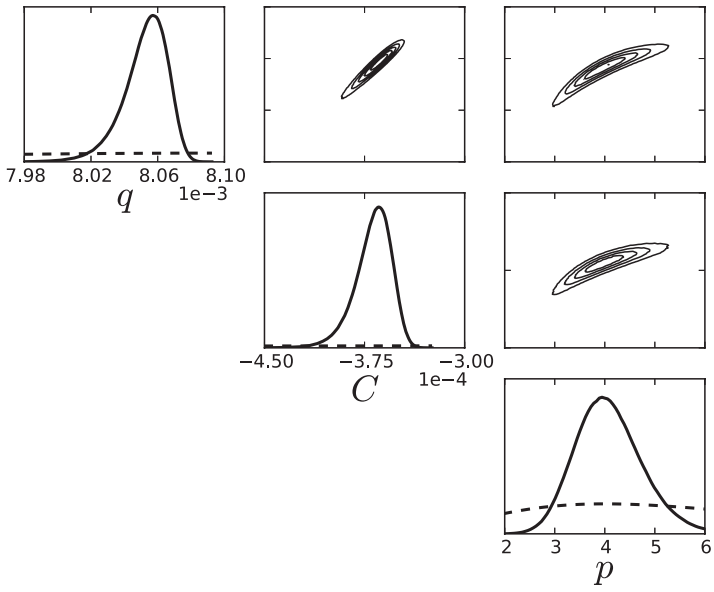

FIG. 7. Results of Bayesian Richardson extrapolation for $q = C_f = 2\tau_w/\rho U_b^2$, C, and p. The input data are C_f from the coarsest, coarse, and nominal meshes for the small domain case. The diagonal shows the marginal prior (dashed line) and posterior (solid line) PDFs for each of the parameters while the off-diagonal contour plots show the joint posterior PDF projected onto planes in parameter space.

Finally, the estimated discretization error on the nominal mesh is shown in Figure 9. As with the centerline velocity, the discretization error is quite small. The mean discretization error is only 0.3% of the mean value. Unlike the centerline velocity, the discretization error is large relative to the estimated sampling error standard deviation, which is less than 0.05%.

3. Summary of results for single-point statistics

Uncertainties in a number of single-point statistics that are generally of interest in DNS are presented here, including the mean velocity, Reynolds stresses, and vorticity variances, as functions of the wall-normal location. As shown for the skin friction and centerline velocity, the first step after performing the Bayesian update to calibrate the discretization error model is to assess the predictions of the model relative to the finest mesh results. Here, this assessment is performed by evaluating the CDF corresponding to the prediction for the finest mesh value, as given by (16), at the observed result for the finest mesh. This value is important because, if it is close to zero or close to one, then the observed value corresponds to a draw from one of the tails of the prediction distribution.

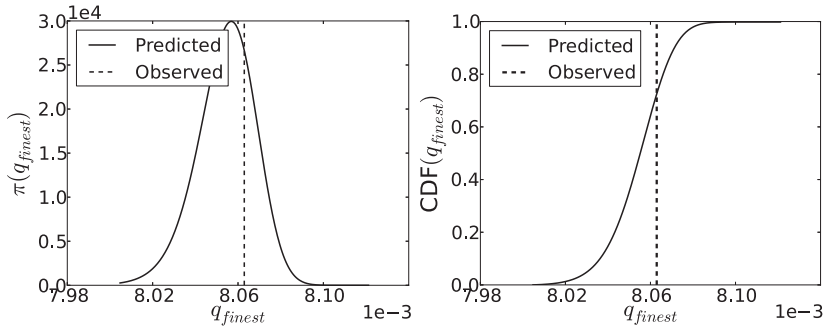

(a) PDF (b) CDF

FIG. 8. Prediction distribution of the mean skin friction coefficient for the finest mesh using (16) and the observed mean skin friction computed on the finest mesh for the small domain case.

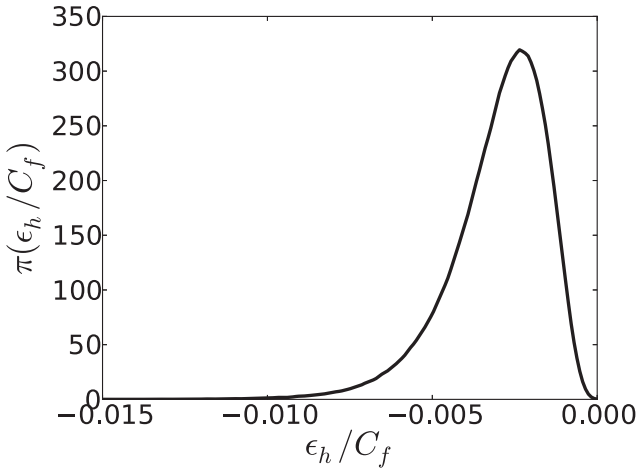

FIG. 9. Distribution of estimated discretization error in the skin friction on the nominal mesh for the small domain case, as determined by Bayesian Richardson extrapolation.

The results are presented in Figure 10. In each figure, the solid line is the computed value of the CDF at the observed value. The gray region shows the region between 0.05 and 0.95, which is the 90% credibility interval. When the observed results give a CDF value that falls outside of this region, the model and the observation are in poor agreement. In this case, we cannot have confidence in the model, and it is declared invalid for our purposes. When the values are in the gray region, the model passes this validation check.

For the mean velocity, viscous stress, Reynolds shear stress, wall-normal velocity variance, and spanwise velocity variance, there is reasonable to excellent agreement between the model predictions and the observations. For these quantities, the model is not invalidated by this assessment. Alternatively, for the streamwise velocity variance and the vorticity variances, there are large regions of the channel where the observed value falls outside of the 90% credibility interval. For example, examining $\langle u'u' \rangle$, for $50 \lesssim y^+ \lesssim 100$, the percentile of the observed value is greater than 95%, meaning that the model assigns probability greater than 0.95 to values smaller than the observed value. This level of disagreement means that the model cannot be used with confidence. The model for the vorticity variances is also invalid based on this assessment.

A closer examination of the $\langle u'u' \rangle$ data for $50 \lesssim y^+ \lesssim 100$ shows the problem. The results are not converging monotonically with increasing mesh resolution. For example, at $y^+ \approx 62$, the value of $\langle u'u' \rangle / U_b^2$ on the coarsest, coarse and nominal meshes was 0.010343, 0.010042, and 0.00997, respectively. However, the value observed on the finest mesh was 0.010010, an increase in magnitude compared to the nominal mesh. This non-monotonic behavior cannot be captured by the simple model used here. By retaining additional terms in the Taylor series expansion (5), as mentioned in Sec. II B 2, one could formulate a model capable of producing non-monotonic convergence. However, we do not investigate such models here because they introduce additional parameters that must be informed by data. With only the data available for calibration here—i.e., the three coarser mesh results—it is not possible to inform all these parameters, meaning that some would be constrained only by prior information. Since no specific information regarding the behavior of the discretization error outside the asymptotic regime is available, extrapolations to smaller h that are sensitive to such prior information cannot be trusted. It would be possible to learn the true non-monotonic behavior if more data were available for calibration and validation of the discretization error model, but this is beyond the scope of the current work. Non-monotonic behavior is also present in the vorticity variance data, and the discretization error model also fails the validation test for the vorticity variances.

Thus, it is clear that the simple model used here is insufficient for some quantities. Given that the complete discretization is a mix of spectral, high-order B-spline, and 2nd and 3rd order time marching schemes, it is not surprising that the convergence behavior is complex, and in fact none of the results are consistent with the final asymptotic behavior of the scheme, which must be 2nd

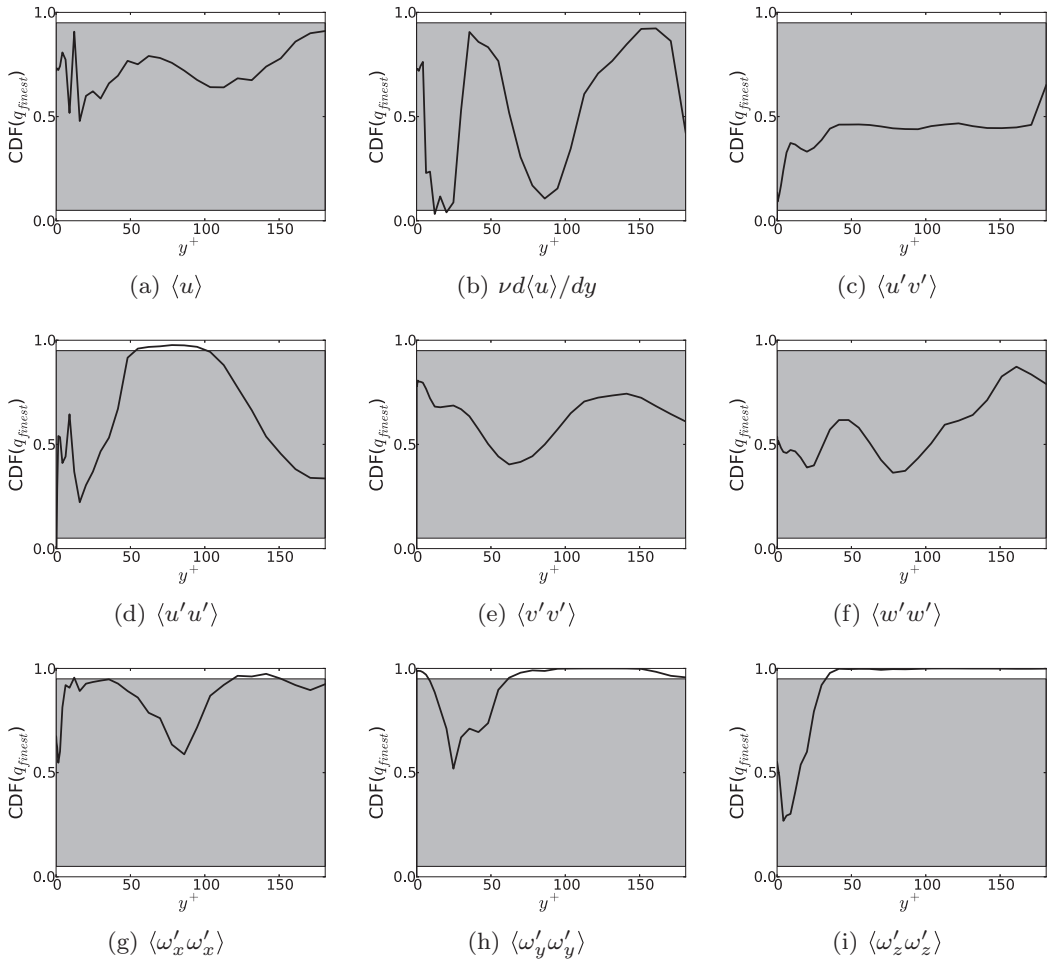

FIG. 10. Value of the prediction CDF at the observed value on the finest mesh, as determined by Bayesian inference using the small domain results. When this value is <0.05 or >0.95, the observation is on the tail of the prediction PDF, indicating disagreement between the prediction and the observation.

order due to the temporal discretization of the viscous terms. It is important to understand that the invalidity of the discretization error model for some quantities implies nothing whatsoever about the sufficiency of the discretization resolution or the averaging time interval. This validation failure shows only that the discretization error is not in the asymptotic regime. This fact may be because the mesh is not yet sufficiently resolved to show asymptotic behavior for any component of the error. Or, it may be because the dominant error changes between the meshes. For instance, the spatial error may dominate on the coarsest mesh but, because it is higher order than then temporal error, not on the nominal mesh. In such a case, the effective order is changing with h, which would cause our model to be invalid. Regardless, the fact that an error is not in the asymptotic regime and that our model is invalid does not imply that it is large. For example, the change between the nominal and finest mesh results for $\langle u'u' \rangle / U_b^2$ is less than 0.5%. However, for quantities where the model is invalid, we clearly cannot use it to make reliable statements about the discretization error. For this reason, no additional results are shown for the streamwise velocity variance or vorticity variances.

For the quantities where the model is not invalidated, we use it to predict the discretization error for the nominal mesh result. Figures 11 and 12 show these predictions. The median prediction is shown as a solid line with error bars indicating the 90% credibility interval. For comparison, the estimated sampling error is indicated by the dashed lines, which correspond to the 90% credibility interval of the sampling error model. For all quantities, the errors are presented as percentage values.

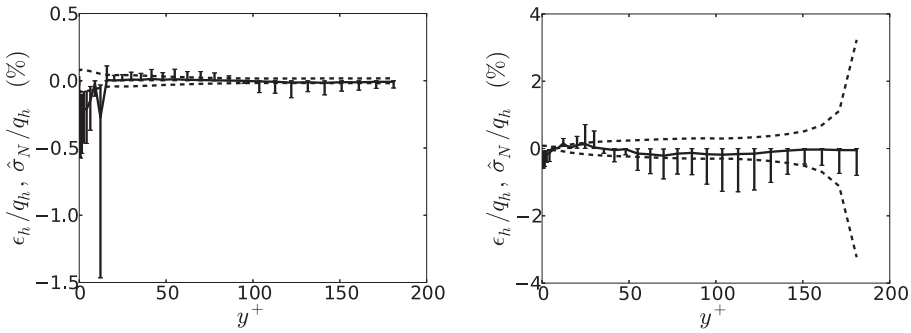

FIG. 11. Estimated discretization error (solid line) and sampling uncertainty (dashed line) for the small domain case. For the discretization error, the curve is the 50 percentile and the error bars indicate the 5th and 95th percentiles. For the sampling uncertainty, the curves represent the 5th and 95th percentiles.

For the mean velocity and viscous shear stress, both the estimated discretization error and sampling errors are less than 1% in magnitude everywhere across the channel. In fact, for most points, the median error in the mean velocity is less than one quarter of a percent, with nearly all the 90% confidence intervals at less than one half of a percent.

Very near the wall, the discretization errors are estimated to be larger than the sampling error. For $y^+ \gtrsim 15$, the median of the discretization error lies within the 90% credibility interval for the sampling error, but generally there is some probability that the discretization error is larger. On the whole, it appears that neither error is dominant.

Qualitatively similar conclusions can be drawn for $\langle u'v' \rangle$, $\langle v'v' \rangle$, and $\langle w'w' \rangle$, but the errors are somewhat larger. The median discretization error is less than 3% everywhere and is only that large near the wall, where these quantities are very close to zero. Near the wall, the discretization error is larger than sampling error. Near the center of the channel, the situation is reversed.

C. Large domain results

Turbulent channel flow simulations at $Re_\tau \approx 180$ have been performed many times. Currently, one of the most useful simulations is that of Hoyas and Jiménez,[53] because of its large spatial domain, because statistical data are easily accessible online, and because it is part of a series of simulations with Reynolds numbers ranging over an order of magnitude. The large domain simulations reported in this subsection were performed in the same domain size ($L_x = 12\pi$, $L_z = 4\pi$) as Hoyas and Jiménez[53] so that a direct comparison can be made to those results, and so that the uncertainty estimates developed here will be indicative of the uncertainties in this commonly referenced work.

Unlike the smaller box case, only three meshes were used, so it is not possible to test the validity of the calibrated discretization error model against a higher resolution result. However,

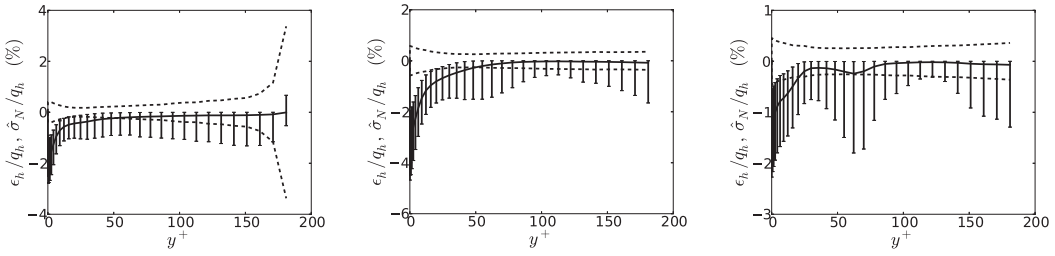

FIG. 12. Estimated discretization error (solid line) and sampling uncertainty (dashed line) for the small domain case. For the discretization error, the curve is the 50 percentile and the error bars indicate the 5th and 95th percentiles. For the sampling uncertainty, the curves represent the 5th and 95th percentiles.

since the Reynolds number and mesh resolution are the same or similar to the small domain case, we expect that the model is valid for the same quantities. Further, consistent with typical DNS practice, statistics were gathered over only a modest simulation time (10s of flow-throughs), although each flow-through with the large box represents significantly more data than the small box case. Full details of the simulation are given in Table II.

1. Centerline mean velocity and skin friction

As in Secs. III B 1 and III B 2, we present detailed results for the centerline mean velocity and the skin friction. The posterior PDFs for the calibration parameters are qualitatively similar to the results for the small domain (see Figures 4 and 7), and are therefore not shown. The posterior PDFs are marginally less well informed due to the somewhat larger sampling uncertainty in the large domain results, but do not differ materially. For example, for the centerline velocity, the true value shifts slightly to the left to a mean of approximately 1.162769, and there is still significant uncertainty about the value of p. The mean is 4.82, but the 5th and 95th percentiles lie at 3.19 and 7.06, respectively. As in the small domain case, the order of accuracy for the skin friction is somewhat better informed than that for the centerline velocity, but there is still significant uncertainty, with the 5th and 95th percentiles at 3.55 and 5.10, respectively. However, the marginal posterior for the true value of C_f is again quite narrow, with the difference between the 5th and 95th percentiles being only 0.54% of the mean value.

Figure 13 shows the estimated discretization error for the centerline velocity on the nominal mesh, normalized by the observed mean value. As in the small box case, it is almost certain that the discretization error is less than 0.1%, and the mean is only 0.026%. The 50th percentile lies at approximately 0.021%, which is very close to the estimated standard deviation of the sampling error.

The estimated discretization error in the skin friction on the nominal mesh is shown in Figure 14. As in the small box case, the discretization error is small, with a mean of approximately 0.24%. For comparison, the estimated standard deviation of the sampling error is approximately 0.092%.

As mentioned earlier, this domain size is identical to that of a previous $Re_\tau \approx 180$ simulation reported by Hoyas and Jiménez.[53] For the purposes of verification, a direct comparison between that simulation and the nominal mesh of this study is performed. The centerline velocity on the nominal mesh for our study is 1.16303 ± 0.00025 where the quoted uncertainty estimate is one standard deviation of the sampling error. This is within 0.031% of the value of 1.16267 quoted by Hoyas and Jiménez.[53] While small, these values differ by more than a standard deviation of the estimated sampling error. However, these two simulations, while run with similar resolution, did differ in both

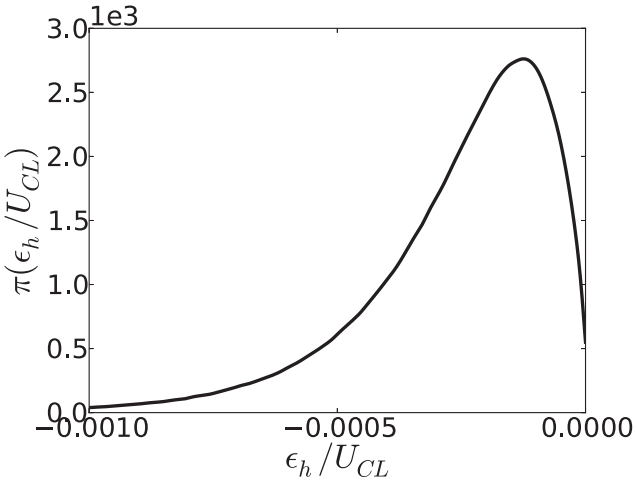

FIG. 13. Distribution of estimated discretization error in the centerline velocity on the nominal mesh for the large domain case, as determined by Bayesian Richardson extrapolation.

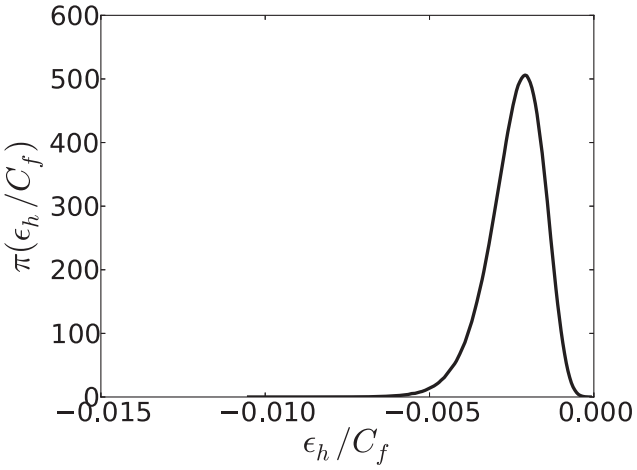

FIG. 14. Distribution of estimated discretization error in the skin friction on the nominal mesh for the large domain case, as determined by Bayesian Richardson extrapolation.

their choice of wall-normal numerics (B-splines vs. Chebychev polynomials) as well as the number of points in y (128 vs. 97). It is therefore plausible that the discrepancy between the values of the centerline velocity in these simulations is a combined result of discretization error and sampling error. Indeed, the observed difference of 0.00036 is in the range of plausible discretization errors ϵ_h, as shown in Figure 13. Similarly, our value of the skin friction coefficient from the nominal mesh ($0.00807834 \pm 7.49 \times 10^{-6}$) differs by ≈0.4% from the value quoted by Jiménez ($0.00811666 \pm 3.4 \times 10^{-7}$). In absolute terms, this is a very small difference, but it is significantly larger than the estimated sampling error. Recalling the aforementioned differences between the present wall-normal numerics and those of Hoyas and Jiménez,[53] it is plausible that the discrepancy is due to discretization error. Indeed, the ≈0.4% discrepancy is plausible as a value of the discretization error as shown in Figure 14.

2. Summary of results for single-point statistics

This section shows the estimated discretization and sampling errors for the mean velocity $\langle u \rangle$, viscous shear stress $\nu d\langle u \rangle/dy$, Reynolds shear stress $\langle u'v' \rangle$, wall-normal velocity variance $\langle v'v' \rangle$, and spanwise velocity variance $\langle w'w' \rangle$. Recall that the discretization error model for these quantities passed the validation assessment for the small domain case, as shown in Sec. III B 3.

The results are shown in Figures 15 and 16, which are analogous to Figures 11 and 12 for the small domain results. As in the small domain case, the estimated discretization errors in the mean

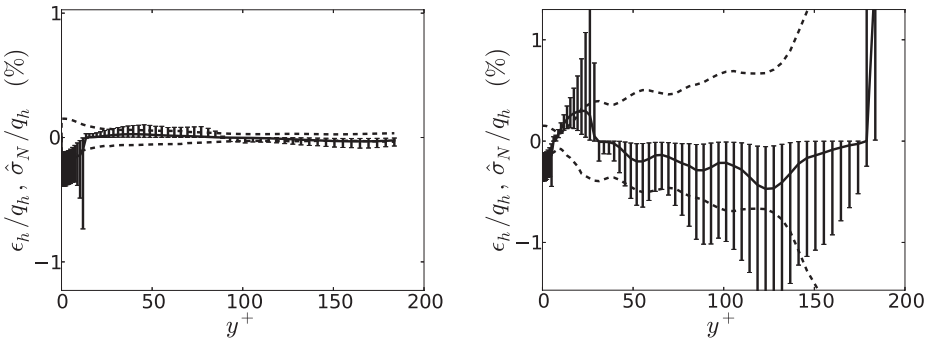

(a) $\langle u \rangle$ (b) $\nu d\langle u \rangle/dy$

FIG. 15. Estimated discretization error (solid line) and sampling uncertainty (dashed line) for the large domain case. For the discretization error, the curve is the 50 percentile and the error bars indicate the 5th and 95th percentiles. For the sampling uncertainty, the curves represent the 5th and 95th percentiles.

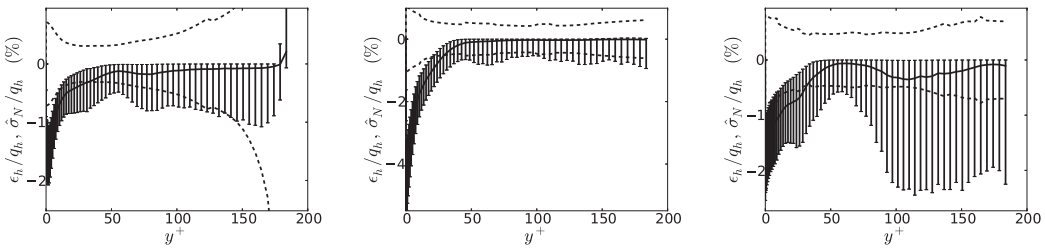

(a) $\langle u'v' \rangle$ (b) $\langle v'v' \rangle$ (c) $\langle w'w' \rangle$

FIG. 16. Estimated discretization error (solid line) and sampling uncertainty (dashed line) for the large domain case. For the discretization error, the curve is the 50 percentile and the error bars indicate the 5th and 95th percentiles. For the sampling uncertainty, the curves represent the 5th and 95th percentiles.

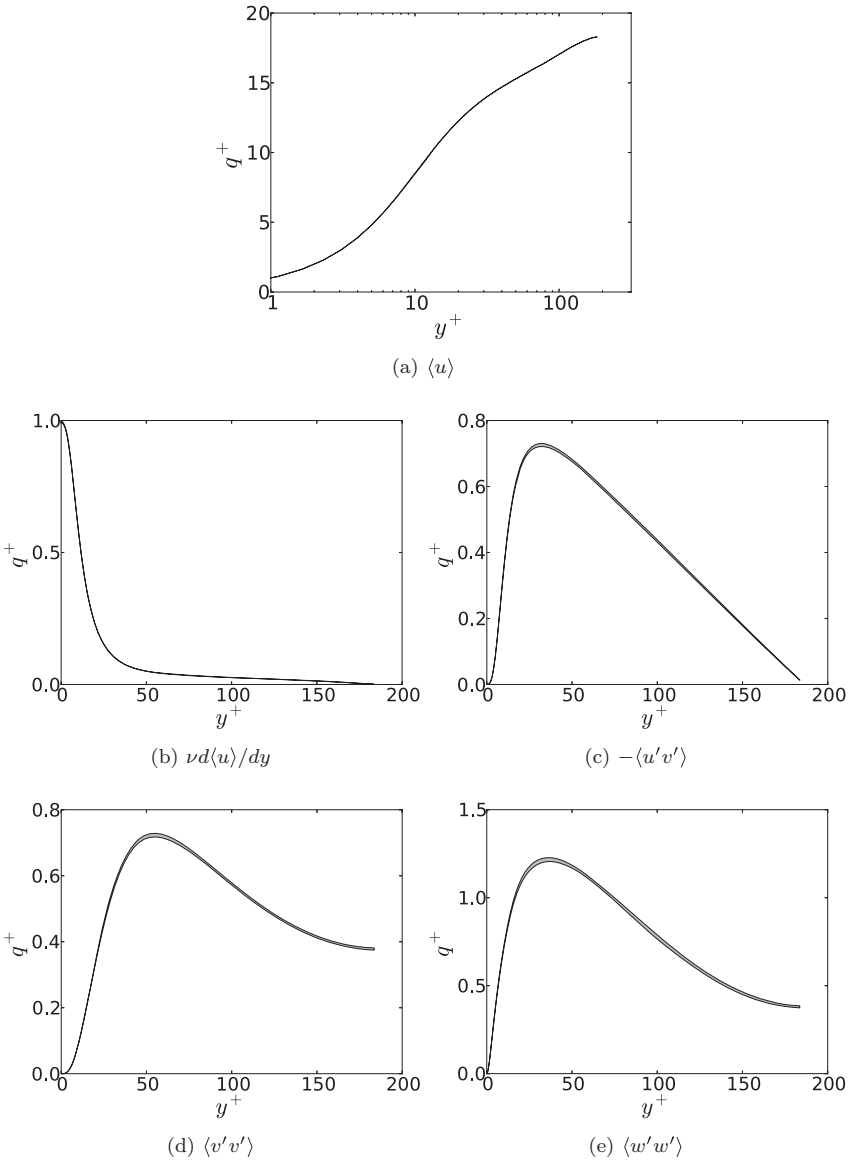

(a) $\langle u \rangle$

(b) $\nu d\langle u \rangle/dy$ (c) $-\langle u'v' \rangle$

(d) $\langle v'v' \rangle$ (e) $\langle w'w' \rangle$

FIG. 17. Estimated true value obtained from the posterior distribution for q based on the large domain results. The gray region shows the 90% credibility interval between the 5th and 95th percentiles of the posterior. All quantities are normalized using the nominal value of u_τ.

velocity and viscous stress are less than one percent nearly everywhere. The larger percentage errors in the viscous stress near the centerline are an artifact of the local viscous stress going to zero at the center of the channel. The largest percent error observed anywhere aside from the centerline is roughly four percent in $\langle v'v' \rangle$ very near the wall. Of course, $\langle v'v' \rangle \propto y^4$ as $y \to 0$, meaning that this error is still very small. Finally, in general, the discretization errors observed are largest near the wall. In this region, they tend to be larger than the sampling error. In the center of the channel, the sampling error is generally larger.

In addition to providing an assessment of the discretization error on the nominal mesh, the Bayesian procedure provides an estimate of the true value in the limit of infinite resolution ($h \to 0$). This estimate is provided by the posterior distribution for q that is obtained from the Bayesian update that is performed to calibrate the discretization error model. These posterior estimates for the true profiles are plotted in Figure 17 for the quantities for which the discretization error model was found valid for the small domain results.

All quantities are plotted using wall normalization, but, to avoid introducing additional uncertainty due to the fact that u_τ is an uncertain quantity, the nominal value for u_τ is used. The resulting intervals are small. For mean velocity and viscous shear stress, the uncertainty is small enough that the 90% credibility interval appears as just a thick line. In the Reynolds stress and wall-normal and spanwise variances, the effect of the uncertainty is more visible, particularly near the peak values, but still quite small.

IV. CONCLUSIONS

DNS data are crucial to advancing understanding of turbulent flow physics and to calibration of engineering models of turbulent flow. Given these uses, it is important to fully understand and characterize the errors and uncertainties in computed statistical outputs. However, because of complications due to sampling error, systematic studies of discretization error are not standard for DNS. In this work, two enabling utilities have been developed and applied: a sampling error estimator that accounts for correlation in the data used to compute statistics and a Bayesian extension of Richardson extrapolation that can be used to estimate discretization error in the presence of uncertainty due to finite sampling. These tools enable systematic estimation of both sampling and discretization errors in statistical quantities computed from simulations of chaotic systems.

The results for the Lorenz equations demonstrate that these tools perform well in a simple, well-understood setting. However, the results for DNS of $Re_\tau = 180$ channel flow indicate that their usage in a complex setting is more difficult. One obvious complication is that discretization errors resulting from practical simulations may not be in the asymptotic regime. The simple discretization error representation used here was found to be adequate for many important quantities, including mean velocity and Reynolds shear stress. Further, the estimated errors in these quantities are small, indicating that the usual heuristics used to design meshes for DNS of wall-bounded turbulence are reasonable. Thus, we conclude that simulations of higher Reynolds number channel flow based on these resolution heuristics with similar sampling time, such as those reported by Jiménez and co-workers,[16,44,45,53] can be expected to have errors of the same magnitude as those reported here.

However, for other quantities, most notably the streamwise velocity variance, the discretization error model is invalidated by comparison against higher resolution simulations than those used to calibrate the model. Due to this failure, we are unable to quantify the discretization error in these quantities with confidence. Nonetheless, the errors appear to be small because the observed change from the nominal to finest resolution results is quite small.

It may be possible to estimate the discretization error in quantities for which the simple discretization error model fails by posing and calibrating a more complex model. Such a model could be based on retaining additional terms in a Taylor series expansion of the discretization error, although proper calibration of this model would require additional simulations beyond those used here. Future work for channel flow should focus on understanding the discretization errors in the quantities for which the simple model was found invalid. Further, the results obtained here cannot be extrapolated to resolution and sampling heuristics used for other numerical schemes or for other classes of flow. Additional studies using the techniques developed here should be pursued for these cases. While it

will likely not be practical to apply the full Bayesian Richardson extrapolation technique for each new simulation, by assessing the relevant resolution heuristics in a computationally tractable setting, as done for low *Re* channel flow here, one can develop estimates of the expected numerical accuracy of the results of more demanding simulations. These estimates can then be combined with sampling error estimates, which are tractable for even expensive DNS, to obtain a complete characterization of DNS uncertainties.

ACKNOWLEDGMENTS

The work presented here was supported by the Department of Energy [National Nuclear Security Administration] under Award No. DE-FC52-08NA28615 and the National Science Foundation under Award No. OCI-0749223.

The authors acknowledge the Texas Advanced Computing Center (TACC) at The University of Texas at Austin for providing HPC resources that have contributed to the research results reported here. Finally, the authors wish to thank Mr. Myoungkyu Lee for the use of his simulation code as well as his assistance in generating several of the DNS runs.

APPENDIX: MOTIVATION FOR THE SAMPLING ERROR ESTIMATOR

If the samples X_i were independent, the classical CLT states that

$$e_N \xrightarrow{d} \mathcal{N}(0, \sigma^2/N),$$

where $\sigma^2 = \mathrm{Var}\, X = E[(X-\mu)^2]$. However, the samples resulting from a DNS calculation have *a priori* unknown correlation structure and, at least for small temporal or spatial separation, are certainly not independent.

To avoid the complications of correlated samples, many authors downsample instantaneous measurements until the retained samples are arguably uncorrelated and then use an estimate based on the classical CLT. However, optimally downsampling autocorrelated samples requires coarsening the data "just enough" to decorrelate the signal but not "too much" to avoid discarding useful data.[18] As increasing the number of independent samples is computationally expensive in DNS, it is imperative to extract all possible information from the data. Thus, we seek a method to estimate the uncertainty in statistics computed from correlated samples.

The method developed in Sec. II A is motivated by an extension of the CLT from a sequence of independent, identically distributed random variables to an α-mixing sequence. For the precise statement of the theorem see Billingsely[54] (Theorem 27.4) or Zhengyan and Chuanrong[55] (Theorem 3.2.1). Loosely speaking, the theorem states that, if random variables "far" apart in the sequence are nearly independent, which is expected for data resulting from DNS, then as $N \to \infty$,

$$e_N \xrightarrow{d} \mathcal{N}(0, s^2/N),$$

where

$$s^2 \equiv E[(X_0-\mu)^2] + 2\sum_{k=1}^{\infty} E[(X_0-\mu)(X_k-\mu)].$$

Thus,

$$\mathrm{Var}\, e_N \to \frac{s^2}{N} = \frac{\sigma^2}{N}\left(1 + 2\sum_{k=1}^{\infty}\rho(k)\right),$$

where

$$\rho(k) = \frac{E[(X_0-\mu)(X_k-\mu)]}{E[(X_0-\mu)^2]},$$

is the autocorrelation at separation k. Thus, the extension for weak dependence simply modifies the effective number of samples from the classical CLT. That is,

$$\operatorname{Var} e_N \to \frac{\sigma^2}{N_{\text{eff}}},$$

where

$$N_{\text{eff}} = \frac{N}{1 + 2\sum_{k=1}^{\infty} \rho(k)}.$$

[1] P. Moin and K. Mahesh, "Direct numerical simulation: A tool in turbulence research," Annu. Rev. Fluid Mech. **30**, 539–578 (1998).
[2] J. Jiménez and R. D. Moser, "What are we learning from simulating wall turbulence?" Philos. Trans. R. Soc., A **365**, 715–732 (2007).
[3] G. Alfonsi, "On direct numerical simulation of turbulent flows," Appl. Mech. Rev. **64**, 020802 (2011).
[4] S. B. Pope, *Turbulent Flows* (Cambridge University Press, 2000).
[5] D. C. Wilcox, *Turbulence Modeling for CFD*, 3rd ed. (DCW Industries, 2006).
[6] P. A. Durbin and B. A. Pettersson Reif, *Statistical Theory and Modeling for Turbulent Flows* (Wiley, 2011).
[7] S. H. Cheung, T. A. Oliver, E. E. Prudencio, S. Prudhomme, and R. D. Moser, "Bayesian uncertainty analysis with applications to turbulence modeling," Reliab. Eng. Sys. Saf. **96**, 1137–1149 (2011).
[8] T. A. Oliver and R. D. Moser, "Bayesian uncertainty quantification applied to RANS turbulence models," J. Phys.: Conf. Ser. **318**, 042032 (2011).
[9] AIAA Committee on Standards, "AIAA guide for verification and validation of computational fluid dynamics simulations," AIAA Paper 98-G-077, 1998.
[10] American Society of Mechanical Engineers, "Guide for Verification and Validation in Computational Solid Mechanics" (ASME V&V 10, 2006).
[11] P. J. Roache, *Verification and Validation in Computational Science and Engineering* (Hermosa Publishers, 1998).
[12] C. J. Roy, "Review of code and solution verification procedures for computational simulation," J. Comput. Phys. **205**, 131–156 (2005).
[13] W. L. Oberkampf and C. J. Roy, *Verification and Validation in Scientific Computing* (Cambridge University Press, 2010).
[14] P. E. Kloeden and E. Platen, *Numerical Solution of Stochastic Differential Equations* (Springer-Verlag, 1992).
[15] D. A. Donzis, P. K. Yeung, and K. R. Sreenivasan, "Dissipation and enstrophy in isotropic turbulence: Resolution effects and scaling in direct numerical simulations," Phys. Fluids **20**, 045108 (2008).
[16] S. Hoyas and J. Jiménez, "Reynolds number effects on the Reynolds-stress budgets in turbulent channels," Phys. Fluids **20**, 101511 (2008).
[17] K. E. Trenberth, "Some effects of finite sample size and persistence on meteorological statistics. Part I: Autocorrelations," Mon. Weather Rev. **112**, 2359–2368 (1984).
[18] F. W. Zwiers and H. von Storch, "Taking serial correlation into account in tests of the mean," J. Clim. **8**, 336–351 (1995).
[19] P. M. T. Broersen, "Automatic spectral analysis with time series models," IEEE Trans. Instrum. Meas. **51**, 211–216 (2002).
[20] P. M. T. Broersen, *Automatic Autocorrelation and Spectral Analysis* (Springer–Verlag, 2006).
[21] C. Chatfield, *The Analysis of Time Series: An Introduction* (Chapman & Hall/CRC, 2004).
[22] D. B. Percival, "Three curious properties of the sample variance and autocovariance for stationary processes with unknown mean," Am. Stat. **47**, 274–276 (1993).
[23] H. von Storch and F. W. Zwiers, *Statistical Analysis in Climate Research* (Cambridge University Press, 2001).
[24] G. E. P. Box, G. M. Jenkins, and G. C. Reinsel, *Time Series Analysis: Forecasting and Control*, 4th ed. (John Wiley, 2008).
[25] M. B. Priestley, *Spectral Analysis and Time Series: Univariate Series* (J. W. Arrowsmith, 1981), Vol. 1.
[26] P. M. T. Broersen, "Finite sample criteria for autoregressive order selection," IEEE Trans. Signal Process. **48**, 3550–3558 (2000).
[27] J. P. Burg, "Maximum entropy spectral analysis," Ph.D. thesis (Stanford University, 1975).
[28] N. Andersen, "Comments on the performance of maximum entropy algorithms," Proc. IEEE **66**, 1581–1582 (1978).
[29] L. J. Faber, "Commentary on the denominator recursion for Burg's block algorithm," Proc. IEEE **74**, 1046–1047 (1986).
[30] N. Andersen, "On the calculation of filter coefficients for maximum entropy spectral analysis," Geophys. **39**, 69–72 (1974).
[31] P. Strobach, "Pure order recursive least-squares ladder algorithms," IEEE Trans. Acoust., Speech, Signal Process. **34**, 880–897 (1986).
[32] J. W. Eaton, D. Bateman, and S. Hauberg, *GNU Octave Manual Version 3* (Network Theory Limited, 2008).
[33] F. L. Drake and G. Rossum, *The Python Language Reference Manual* (Network Theory Ltd., 2011).
[34] R. T. Cox, *The Algebra of Probable Inference* (Johns Hopkins University Press, 1961).
[35] R. P. Christian, *The Bayesian Choice* (Springer, 2001).
[36] E. T. Jaynes, *Probability Theory: The Logic of Science* (Cambridge University Press, 2003).
[37] J. Kaipio and E. Somersalo, *Statistical and Computational Inverse Problems* (Springer, 2005).
[38] D. Calvetti and E. Somersalo, *Introduction to Bayesian Scientific Computing* (Springer, 2007).
[39] C. Robert and G. Casella, *Monte Carlo Statistical Methods* (Springer, 2010).
[40] D. Foreman-Mackey, D. W. Hogg, D. Lang, and J. Goodman, "emcee: The mcmc hammer," Publ. Astron. Soc. Pac. **125**, 306–312 (2013).

[41] J. Goodman and J. Weare, "Ensemble samplers with affine invariance," Commun. Appl. Math. Comput. Sci. **5**, 65–80 (2010).
[42] O. Tange, "GNU parallel - the command-line power tool," USENIX; login: **36**, 42–47 (2011).
[43] J. Kim, P. Moin, and R. D. Moser, "Turbulence statistics in fully developed channel flow at low Reynolds number," J. Fluid Mech. **177**, 133–166 (1987).
[44] J. C. del Álamo and J. Jiménez, "Spectra of the very large anisotropic scales in turbulent channels," Phys. Fluids **15**, L41–L44 (2003).
[45] J. C. del Álamo, J. Jiménez, P. Zandonade, and R. D. Moser, "Scaling of the energy spectra of turbulent channels," J. Fluid Mech. **500**, 135–144 (2004).
[46] M. Lee, N. Malaya, and R. D. Moser, "Petascale direct numerical simulation of turbulent channel flow on up to 786k cores," in *Proceedings of SC13: International Conference for High Performance Computing, Networking, Storage and Analysis*, SC'13 (ACM, New York, NY, USA, 2013), pp. 61:1–61:11.
[47] P. R. Spalart, R. D. Moser, and M. M. Rogers, "Spectral methods for the Navier-Stokes equations with one infinite and two periodic directions," J. Comput. Phys. **96**, 297–324 (1991).
[48] W. Y. Kwok, R. D. Moser, and J. Jiménez, "A critical evaluation of the resolution properties of B-Spline and compact finite difference methods," J. Comput. Phys. **174**, 510–551 (2001).
[49] R. Johnson, "Higher order B-spline collocation at the Greville abscissae," Appl. Numer. Math. **52**, 63–75 (2005).
[50] O. Botella and K. Shariff, "B-spline methods in fluid dynamics," Int. J. Comput. Fluid Dyn. **17**, 133–149 (2003).
[51] R. Courant, K. Friedrichs, and H. Lewy, "Über die partiellen Differenzengleichungen der mathematischen Physik," Math. Ann. **100**, 32–74 (1928).
[52] P. M. T. Broersen, "Practical aspects of the spectral analysis of irregularly sampled data with time-series models," IEEE Trans. Instrum. Meas. **58**, 1380–1388 (2009).
[53] S. Hoyas and J. Jiménez, "Scaling of the velocity fluctuations in turbulent channels up to $re_\tau = 2003$," Phys. Fluids **18**, 011702 (2006).
[54] P. Billingsely, *Probability and Measure*, 4th ed. (Wiley, 2012).
[55] L. Zhengyan and L. Chuanrong, *Limit Theory for Mixing Dependent Random Variables*, Mathematics and Its Applications, Vol. 378 (Science Press/Kluwer Academic Publishers, 1996).